A Broadband Stripline Technique for Characterizing Relative Permittivity and Permeability

C. P. Gallagher, N. Cole, P. P. Savage, C. McKeever, J. R. Sambles and A. P. Hibbins

***Abstract*—We present a stripline design and calibration method allowing the extraction of relative permittivity of single dielectric samples in the 200 MHz – 50 GHz range. The simultaneous extraction of relative permittivity and permeability is also illustrated by characterizing a set of samples comprising magnetic inclusions over the same frequency range. The calibration method involves the use of seven measurements of the stripline scattering parameters (S-parameters) with different length shorts inserted. From these measurements, it is possible to determine the reflections at the transition regions of the stripline to correct the measured S-parameters for characterization. By quantifying a range of samples with increasing percentage volume filling of barium titanate in polyurethane for the case of dielectric samples, and carbonyl iron powder (CIP) for magnetic samples, this work demonstrates a reliable method for the broadband characterization of composite materials.**

***Index Terms*—Calibration techniques, coaxial, deembedding, device characterization, dieletric measurements, EM composite materials and measurements, impedance matching, instrumentation and measurement techniques, magnetic materials, transmission line theory, vector network analysis.**

I. Introduction

THE STRIPLINE transmission line is well established as a device that allows the electromagnetic characterization of materials [1]. This involves connecting a transmission line to a vector network analyzer (VNA), and measuring the transmitted and reflected signals in the form of S-parameters when samples are inserted into the transmission line. The S-parameters are recorded at a range of frequencies. From this information it is possible to extract the relative complex permittivity and permeability across the frequency range, provided the transmission line supports a transverse electromagnetic mode (TEM). The requirement for the transmission line to support a TEM mode is due to the application of Fresnel theory for extracting electromagnetic properties, and means that the geometry of the transmission line used strongly affects the frequency range over which analysis may be performed. Waveguides and coaxial lines may also be used for transmission line measurements, but they have limitations. Waveguides become multimodal outside a relatively narrow bandwidth, meaning multiple readings with different waveguides and different samples need to be taken to cover a broad range of frequencies [2]–[4]. Waveguides also require larger samples for measurement at low frequencies, meaning a lot of material is required for sample preparation. In contrast, measurements with coaxial transmission lines allow broadband measurements with a single sample, typically up to 18 GHz [5]–[7], but the toroidal shape of the sample causes difficulty in fabrication. The toroidal shape also causes difficulty in ensuring there are no air gaps between the conducting core and the circular inner sample boundary however it is possible to compensate for such air gaps in coaxial measurements by considering a coaxial capacitor model [8]–[10]. By comparison, the planar stripline geometry may cover a wide frequency band with a single sample and a simple geometry. However, obtaining high quality results over a wide range of frequencies requires a substantial amount of care [11]. Above an upper cut-off the stripline does become multimodal, meaning sample characterization is still limited to a specific frequency band, but this upper cut-off is seen at higher frequencies than with other transmission lines as it is easier to scale the size of the stripline down, pushing dimensional resonances higher in frequency. The lower cut-off of a stripline is not an issue.

In this work we present an improvement to not only the design of the stripline transmission line, but also an improvement to calibration techniques for this device. These improvements have allowed the maximum frequency of measurement for the stripline device to be increased from a typical value of around 10 GHz, to 50 GHz. Stripline transmission lines are comprised of a pair of ground planes above and below a central conducting strip, as in Fig. 1. The distance between the ground planes, as well as the width and thickness of the center strip, determine the characteristic impedance of the transmission line [12]. The stripline device is typically connected to a VNA by coaxial cables, meaning there is a necessary transition from coaxial geometry to stripline geometry. The end shape of the central conductor is therefore designed to minimise reflections caused by a mismatch in mode shape and a mismatch in impedances of coaxial line and stripline. This transition is usually formed of an 18 - 20° taper from the radius of the coaxial pin to the final strip width [13]–[16]. There is also a necessary transition from coaxial dielectric region to stripline dielectric region, as the coaxial line is circular and enclosed in metal, whereas the stripline comprises three conducting planes with open sides. This transition from diameter of coaxial line to height of stripline causes a discontinuity which leads to the excitation of non-TEM modes at higher frequencies. The frequency of appearance of these modes is dependent upon the height of the stripline. By matching the height of the

This work was supported by The Engineering and Physical Sciences Research Council (EPSRC) of the United Kingdom and The Defence Science and Technology Laboratory (DSTL) of The United Kingdom, via the EPSRC Center for Doctoral Training in Metamaterials (Grant No. EP/L015331/1). All data created during this research are openly available from the University of Exeter's institutional repository at https://ore.exeter.ac.uk/repository/handle/XXXXX/YYYYY.)

Electromagnetic and Acoustic Materials Group, Department of Physics and Astronomy, University of Exeter, Exeter EX4 4QL, United Kingdom

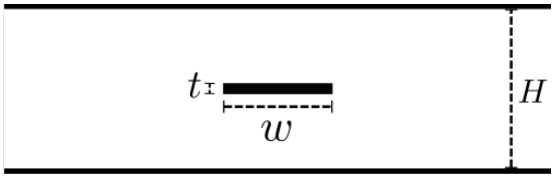

Fig. 1. Cross-section of the stripline geometry, with metal central conductor shown in solid black. The distance between the ground planes, H, width of the line, w and thickness of the line, t, all determine the characteristic impedance of the transmission line.

stripline to the diameter of the coaxial line, it is possible to push the frequency of this cut-off to its upper limit, and prevent other modes from being introduced. The need to match stripline cavity height to coaxial diameter puts a lower bound on the stripline size able to be used, and ultimately leads to a maximum frequency that this device may be used for.

The network analyzer measures S-parameters that represent the whole system, including the transitions from coaxial cable to stripline as well as propagation along the line before reaching the material itself. There are also reflections between the cavity walls and the sample-air interface in the stripline cavity. A calibration is required to de-embed the material S-parameters from those measured. It is possible to compensate for the propagation along the unfilled region of transmission line by simply correcting the phase of the signal. Unwanted reflections at the transition from coaxial line to stripline are compensated for by performing calibrations to determine the S-parameters of the transition regions themselves. To establish these requires measurement of the transmission line S-parameters with known changes to the system or standard impedances inserted. These standards may be 'shorts', 'matched loads', or known changes in transmission line length. A common calibration method used employs measurements of the transmission line with a short, impedance matched load, and open as well as a 'through' measurement of the empty line. This calibration method is known as the SOLT (Short, Open, Load, Through) method, and is typically used for coaxial line calibration [17]. In general, the matched loads allow only the determination of the whole line parameters and the key is to determine a way to compensate for the transition regions between the coaxial lines and the central region of the stripline. This requires an ability to create standards which fit into the cavity of the stripline. A powerful calibration technique has been proposed in [18], where readings with shorts placed at three different positions between the transition regions were used to de-embed the sample S-parameters from the total S-parameters of the transmission line-sample system.

Here we present an improvement to the calibration technique suggested in [18], which allows broadband characterization of the stripline transmission regions, as well as an improved stripline geometry, which gives enhanced impedance matching across broadband frequencies. Both improvements have been employed to extract the relative permittivity of dielectric samples between 200 MHz and 50 GHz. The samples are comprised of barium titanate in a polyurethane matrix with percentage volume loading of $BaTiO_3$ ranging from 0 to 25%. We also present results illustrating the simultaneous extraction

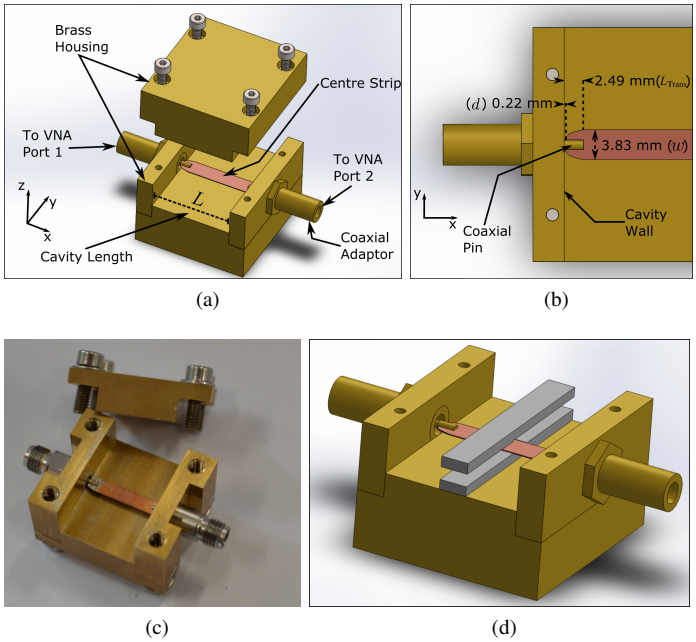

Fig. 2. (a) Schematic showing the stripline geometry. Coaxial adapters screw into the walls of a brass housing, and the center conducting strip is connected using coaxial pins. (b) Close-up image of the transition region from coaxial pin to central strip shape. (c) Photograph of the stripline device. (d) Schematic showing the sample placement in the stripline. Samples are placed above and below the central conductor such that the step in each sample is either side of the line.

of both relative permittivity and permeability across the same frequency range for magnetic samples comprised of carbonyl iron powder (CIP) in polyurethane with percentage volume loading ranging from 10 to 50%.

II. Method

A. Optimization of the Stripline

First the impedance of the improved stripline was optimized by adjusting the shape of the center strip transition regions. Using an electromagnetic model of the ends of the stripline with a general shape comprising 10 vertices, a genetic algorithm was used to minimize the reflection, S_{11}, and maximize transmission, S_{21}. A finite element method (FEM) analysis was utilised for this optimisation, and an in-built optimisation utility was used for applying a genetic algorithm to the objective function. The final geometry converged upon was approximated with a smooth curve that gives the relationship between width, w, of the line, and distance along the line, x. This transition region ends at a given length, L_{Trans}, and is repeated on the opposing end of the strip for transition back to the coaxial adapter.

$$w = \begin{cases} r_0 & \text{for } x \le d \\ r_0 + A\sqrt[3]{x-d} & \text{for } d \le x \le L_{\text{Trans}} \\ 3.83 \text{ mm} & \text{for } x \ge L_{\text{Trans}} \end{cases} \quad (1)$$

Here r_0 is the radius of the coaxial pin, and A is a scaling factor, which when optimised takes a value of 0.01 and x is the distance along the line. Using a stripline geometry with height, H = 3 mm, and cavity length of L = 20 mm the

optimum transition regions begin at a distance, d, from the cavity wall of 0.22 mm and finish at a distance from the cavity wall of $L_{\text{Trans}} = 2.49$ mm. Between the transition regions, the width, w, remains constant at 3.83 mm. Schematics showing the stripline, center strip geometry and sample placement, alongside a photo of the fabricated stripline are shown in Fig. 2. The height, H, between ground planes is set to 3 mm with a central conductor thickness, t, of 0.15 mm. The height of the stripline was chosen to be 3 mm, such that the top and bottom ground planes of the line match the inner diameter of the coaxial adapter.

The dimensions of the cavity for this stripline were changed, such as the length and height. The length of the cavity, provided the transition regions were the same, did not affect the S-parameters of the stripline in models. The height, however, is rather more critical as the 'Short' bars and samples must fit snugly into the stripline as air gaps will cause erroneous data extraction. It was also found that air gaps between the cavity walls and lid of the stripline allow extra non-TEM modes to be excited. These air gaps may be as small as tens of microns and still cause issue in calibration. To minimise the prevalence of these issues, the joins of the lid to the cavity walls were sealed at the bottom with conductive paste, and where air gaps at the top were persistent, toolmaker's clamps were used for sealing.

Other dimensions for the stripline were changed such as the width of center conductor and thickness. This will cause the S-parameters for the stripline to become sub-optimal. Provided no non-TEM modes are able to be supported, the secondary 'Short' calibration accounts for these extra reflections caused by impedance mismatch. The inverse relationship between the frequency at which higher order modes appear and the stripline height was investigated by testing extraction of S-parameters for samples inserted into striplines with the same central conductor but different heights. Each height returned the following result: 3 mm tall stripline operation up to ~ 50 GHz, 10 mm tall operation up to $\sim$ 17 GHz, 15 mm tall operation up to $\sim$ 10 GHz, and 20 mm tall operation up to ~ 5 GHz.

B. Calibration of Transition Regions

As demonstrated in [18], it is possible to account for the influence of the transition regions by using a triple 'short' technique, with conducting metal samples as shorting bars. A minimum of three measurements of the reflected signal with these shorting bars at different positions are required in order to provide enough data to extract the 3 S-parameters of the two transition regions, S_{11}, S_{22} and $S_{21} = S_{12}$. At specific frequencies, the phase of reflected signals measured with 'shorts' at different positions will coincide. The frequency at which this coincidence of phase occurs is related to the position of the shorting bars in each reading. For example, if the shorting bars are placed at a distance l_1 from the cavity end-wall for the first 'short' reading, and at another distance l_2 for the second 'short' reading, the phase of the two 'short' readings will coincide at a frequency simply related to the difference $l_2 - l_1$. When the phase of 'short' readings become similar, the number of datasets available to fit to decrease. With 3 'short' readings to evaluate the transition regions of the stripline, there will not be enough information to accurately describe the transition regions, as when the phase of two of the short readings are the same, there is a degeneracy in the extraction. Because of this failing we have chosen to perform a calibration with 7 'short' readings and fitting together all the 'short' reading data as described below. It is actually sufficient to fit to 4 'short' readings but by taking more, there is less uncertainty in the fit to the modelled system. The equations used to fit to the 'short' readings were formed using a transfer matrix representation of the system. Transfer matrices convert into S-parameters by known relationships [19]. The stripline has two transition regions, A, and B, with a length of uniform line before and after the sample region. It is possible to determine the length of regions either side of the sample or 'short', that is the position of the sample faces, from the difference in phase between the reflected signals S_{11} and S_{22}. These transition regions have their own transfer (T) matrices, which have the following form;

$$\left[T^{\text{A}}\right] = \begin{bmatrix} T_{11}^{\text{A}} & T_{12}^{\text{A}} \\ T_{21}^{\text{A}} & T_{22}^{\text{A}} \end{bmatrix}, \quad \left[T^{\text{B}}\right] = \begin{bmatrix} T_{11}^{\text{B}} & T_{12}^{\text{B}} \\ T_{21}^{\text{B}} & T_{22}^{\text{B}} \end{bmatrix},$$

$$\left[T^{l_n^{\text{A (B)}}}\right] = \begin{bmatrix} \phi_n^{\text{A (B)}} & 0 \\ 0 & \phi_n^{\text{A (B)}^{-1}} \end{bmatrix}, \left[T^{\text{Short}}\right] = \begin{bmatrix} 1 & -1 \\ -1 & 1 \end{bmatrix},$$

where,

$$\phi_n^{\text{A (B)}} = e^{ik_0 l_n^{\text{A (B)}}}, \quad k_0 = \frac{2\pi f}{c},$$

$$L = l_n^{\text{A}} + l_{\text{Sam}} + l_n^{\text{B}}.$$

These transfer matrices multiply to describe the total stripline system;

$$\left[T^{\text{Tot}}\right] = \begin{bmatrix} T_{11} & T_{12} \\ T_{21} & T_{22} \end{bmatrix} = \left[T^{\text{A}}\right] \cdot \left[T^{l_n^{\text{A}}}\right] \cdot \left[T^{\text{Sam}}\right] \cdot \left[T^{l_n^{\text{B}}}\right] \cdot \left[T^{\text{B}}\right]. \tag{2}$$

n is the number index of short reading, and c is the speed of light. When taking 'short' readings, the sample transfer matrix is replaced with T^{Short}. By using equation 2 with T^{Short} inserted and using the relationship $S_{11} = \frac{T_{21}}{T_{11}}$, the reflected signal measured at port 1 may be given in terms of the T-parameters for transition region A and the position of the 'short', embedded in ϕ equation 3,

$$S_{11}^n = \frac{T_{21}^{\text{A}}\phi_n - T_{22}^{\text{A}}\phi_n^{-1}}{T_{11}^{\text{A}}\phi_n - T_{12}^{\text{A}}\phi_n^{-1}}. \tag{3}$$

A sum of least squares fit to all S_{11} readings using equation 3 with 3 complex variables, results in the T-parameters for transition region A. There are only 3 complex variables for each transition region as it is enforced that $S_{21}^{\text{A (B)}} = S_{12}^{\text{A (B)}}$ (Det $\left[T^{\text{A (B)}}\right] = 1$). By fitting to all these 'short' readings as well as those for S_{22} and a measurement of the stripline with no sample inserted, a model of the stripline in terms of T-parameters is produced.

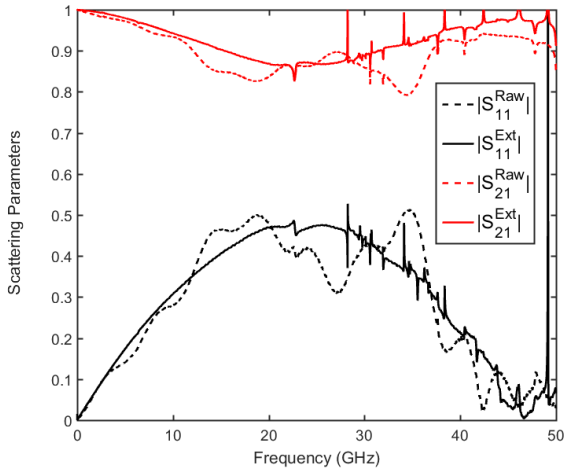

Fig. 3. Comparison of the measured raw S-parameters for the stripline-sample system (dashed lines) and the de-embedded sample S-parameters which have been corrected using our improved calibration technique (solid lines).

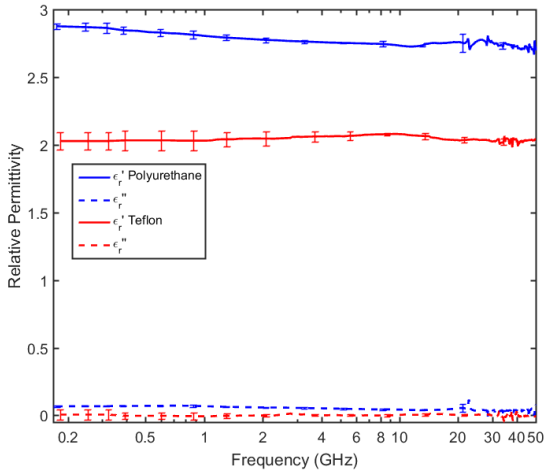

Fig. 4. Relative permittivity for a pure polyurethane sample (Blue) and Teflon sample (Red).

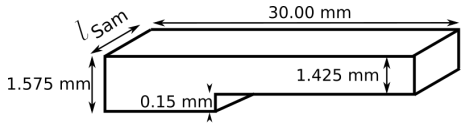

Fig. 5. Schematic showing the dimensions of samples for insertion into the stripline device. Pairs of samples with matching values of l_{Sam} are fabricated for analysis. Schematic is not to scale.

Once the transition region T-parameters are known, they are used to de-embed the sample T-parameters by multiplying the inverses of the transition region T-parameters with those measured with the loaded stripline. These T-parameters may then be converted back to S-parameters. The results for de-embedding the S-parameters of a 2 mm polyurethane sample from the stripline system are shown in Fig. 3. The oscillations found in the original, raw S-parameter data have been calibrated out to give an S-parameter dataset for the polyurethane sample without the influence of the transition regions. The sharp spikes in this S-parameter data are due to artefacts in the calibration process as well as measurement errors. From FEM analysis it was found that a sample width mismatch of 0.5 mm or a 0.5 mm mismatch of sample faces in placement causes sharp resonances in the S-parameter data. This is likely to have carried over from the calibration measurements into the S-parameter extraction. Figure 4 shows the resultant complex permittivity extracted by fitting to the corrected S-parameters measured for Teflon and polyurethane samples.

C. Sample Fabrication

In order to test the design of the proposed stripline, samples were made with increasing index that were either only dielectric, or contained magnetic inclusions for testing simultaneous extraction of permittivity and permeability. Samples were fabricated by mixing dielectric or magnetic powder into a polyurethane resin. The mixture was cast in a mould such that samples may be formed with a 0.15 mm indent to accommodate the central conducting line, allowing complete filling of the cross-section of the cavity. By forming samples in this way, it is possible to create a slab of material from which many sample pairs of the shape in Fig. 5 may be cut with specific values for l_{Sam}. This allows characterization of samples with different lengths, which is useful when characterizing samples with low loss. (When characterizing samples with low loss, the value of S_{11} at Fabry Perot resonances reduces to zero, leading to a degenerate system and inaccuracies in parameter extraction). By measuring multiple lengths of sample, it is possible to overcome this issue by fitting to multiple readings for different thicknesses of samples simultaneously.

Dielectric composite samples were formed with percentage volume fillings of $BaTiO_3$ ranging from 0% vol. to 25% vol. in 5% vol. increments. (The $BaTiO_3$ was obtained from Sigma Aldrich, where the given particle size was ≤ 3 μm.) Magnetic composite samples were formed with percentage volume fillings of CIP ranging from 0% vol. to 40% vol. in 10% vol. increments. The carbonyl iron used was grade CIP ES from BASF with a particle size range 3.0 – 4.0 μm, as stated by BASF. CIP particles tend to be spherical and had a smaller size distribution, meaning the mixture in resin was less viscous than with $BaTiO_3$ particles, thus a higher percentage volume filling was reached. The densities of these samples as a function of percentage volume filling are shown in Fig. 6.

D. Measurement Process

Measurements were taken using the following procedure:

- Perform standard SOLT cable calibration with VNA;
- Take 7 readings of S_{11} and S_{22} with 'shorts' placed at known different positions;
- Measure empty stripline S-parameters;
- Fit (2), (3) to all 'short' readings and empty stripline readings to extract transition region S-parameters;
- Measure stripline S-parameters with sample inserted;
- Use transition region S-parameters to extract sample S-parameters;
- Fit to sample S-parameters with Fresnel theory to find values for relative permittivity and permeability.

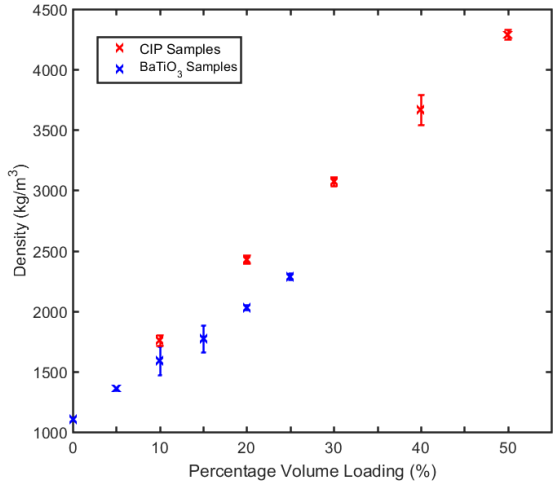

Fig. 6. Measured densities of CIP ES – Polyurethane (red) and $BaTiO_3$ – Polyurethane (blue) composites for each percentage volume loading.

The cables used to connect the stripline to the VNA were 2 ft. long, 2.4 mm (V-Type) cables. The coaxial adapters from circular to stripline geometry were 2.92 mm - 2.4 mm adapters (K-Type to V-Type).

E. Parameter Extraction

In order to extract the relative permittivity and permeability from measured S-parameters for samples, Fresnel theory is implemented. This theory assumes a plane TEM wave propagating through a three-layer system. The three layers are considered to be an air region either side of the sample itself. These air regions account for the propagation along the constant-width section of the line. The air regions also allow for compensation of non-central placement of the sample. The S-parameters for this system are formulated using the transfer matrix approach. Here, a series of matrices represent the reflection and transmission at the sample-air interfaces as well as the propagation along the air and sample regions. The three-layer system may be written in the following form:

$$\left[T^{\text{Fres}}\right] = \tfrac{1}{\tau\tau'}\begin{bmatrix}\phi_{\text{A}} & 0\\ 0 & \phi_{\text{A}}^{-1}\end{bmatrix}\begin{bmatrix}1 & \rho\\ \rho & 1\end{bmatrix}\begin{bmatrix}\phi & 0\\ 0 & \phi^{-1}\end{bmatrix}\begin{bmatrix}1 & -\rho\\ -\rho & 1\end{bmatrix}\begin{bmatrix}\phi_{\text{B}} & 0\\ 0 & \phi_{\text{B}}^{-1}\end{bmatrix}$$

From this set of matrices and using the common relations between T-parameters and S-parameters, it is possible to give a set of equations for S_{11} and S_{21} in terms of the relative permittivity and permeability of the sample;

$$S_{11} = \frac{\rho\phi_A^{-2}(\phi - \phi^{-1})}{(\phi - \rho^2\phi^{-1})} \tag{4}$$

$$S_{21} = \frac{\tau\tau'}{\phi_{\text{A}}\phi_{\text{B}}(\phi - \rho^2\phi^{-1})} = S_{12} \tag{5}$$

where,

$$\rho = \frac{Z-1}{Z+1},$$

$$\tau = \frac{2Z}{Z+1}, \qquad \tau' = \frac{2}{Z+1},$$

$$\phi_{\text{A (B)}} = e^{ik_0 l_{\text{A (B)}}}, \qquad \phi = e^{ik_0 l_{\text{Sam}} n_{\text{Sam}}},$$

$$Z = \sqrt{\frac{\mu_r^*}{\epsilon_r^*}}, \qquad n_{\text{Sam}} = \sqrt{\epsilon_r^*\mu_r^*},$$

$$\epsilon_r^* = \epsilon_r' + i\epsilon_r'', \qquad \mu_r^* = \mu_r' + i\mu_r''.$$

These equations are used to fit to the corrected S-parameters measured with the stripline device. By fitting to a section of frequency at a time, it is possible to extract a value for permittivity and permeability that is then used for the fit to subsequent sections as a function of frequency. This 'Sliding Window Fresnel Fit' was introduced in [13]. The ability to fit to a window of data rather than using single points allows the sharp 'spikes' in the extracted S-parameter data to be removed. (These 'spikes' are artefacts from the extraction process).

F. Sample Placement

Samples are placed into the stripline above and below the central conductor in the orientation shown in Fig. 2(d).

The position of the sample in the stripline may be determined from the phases of the reflected signals from either side of the sample, $\phi_{11}^{\text{Measured}}$ and $\phi_{22}^{\text{Measured}}$. This allows the l_{A} and l_{B} to be determined directly from measurement. If the sample is placed centrally in the stripline, the phases of the reflections would match as the distance travelled by the reflected signals is the same. If the sample is off-center, the signals will have a discrepency in phase related to the difference in distance from each sample wall to each sample-air interface.

In order to determine this offset, a code is used that takes the phase of the measured S_{11} and S_{22} and applies the phase corrections Eq. (6) & (7). The code then adjusts the phase factor until $\phi_{11}^{\text{Corrected}} = \phi_{22}^{\text{Corrected}}$ at which point, l_{A} has been found.

$$\phi_{11}^{\text{Corrected}} = \phi_{11}^{\text{Measured}} + 2k_0 l_{\text{A}} \tag{6}$$

$$\phi_{22}^{\text{Corrected}} = \phi_{22}^{\text{Measured}} + 2k_0(L - l_{\text{Sam}} - l_{\text{A}}) \tag{7}$$

This method is also used for the positioning of shorting bars in the stripline.

III. Results

The results for the relative permittivity of dielectric loaded samples, extracted by fitting Fresnel theory to sample S-parameters with the relative permeability fixed at unity, are shown in Fig. 7.

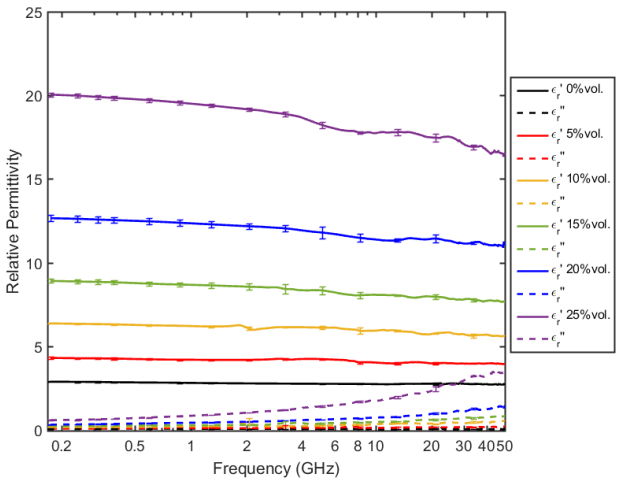

Fig. 7. Relative complex permittivity for $BaTiO_3$ – Polyurethane composites with increasing percentage volume of $BaTiO_3$.

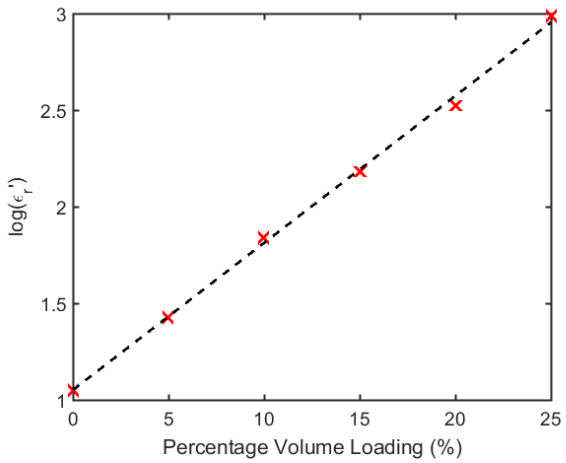

Fig. 8. Natural log of the real part of relative permittivity at 200 MHz for $BaTiO_3$ – Polyurethane composites with increasing percentage volume of $BaTiO_3$. The dashed line shows a linear fit to the data.

The relative permittivity shows an approximately linear dependence on the logarithm of the frequency, as is expected for a dielectric material [20]–[23]. In addition, the relative permittivity of samples at low frequency (200 MHz) increases logarithmically with % volume loading Fig. 8. The logarithmic increase in permittivity with percentage volume loadings agrees with the simple Lichtenecker mixing equation for a relative real permittivity of $BaTiO_3$ of 5700, and for polyurethane of 2.86 [24]. These values were found by fitting to the static values of the logarithm of real permittivity as a function of percentage loading. There is a weak oscillation in the data, which can be caused by a multitude of issues. From modelling it has been seen that if the samples are mismatched in width by 0.5 mm or mismatched in placement, the phases of the two reflected signals will not match, specifically at $\frac{\lambda}{2}$ frequencies. This leads to an error in extraction that brings about these oscillations. The roughness or shape of sample at one face can also differ from the other side, which will also result in oscillations in the extracted data corresponding to $\frac{\lambda}{2}$ frequencies. Much care is taken to ensure sample dimensions are all square but there will inevitably be errors. The analysis of the randomised errors from sample placement, shape mismatch and size mismatch was performed by taking multiple measurements of samples before averaging between different samples and taking the standard deviation. At higher volume loadings, the impedance and loss of samples is such that the magnitude of S_{21} becomes close to zero at high frequencies. This introduces an increased error at higher frequencies for extractions of permittivity and permeability.

There is also a systematic error associated with the height of samples not completely filling the cavity of the stripline. This will have a similar effect to coaxial measurements in that the extracted permittivity of samples will appear low. Samples were cast in a mould such that their height is accurate to within 20 μm and silver conductive paste was painted on the faces of the samples touching the outer conductors to remove the source of systematic error. However, there may also be air gaps between samples at the central conductor and between the sample interfaces at the center. These errors are difficult to estimate due again to roughness of the samples however it is known that the error will reduce the permittivity. It is also difficult to remove air gaps between sample interfaces at the center of the line, as conductive paste may not be used to seal these gaps. The permeability is affected less by air gaps at the top and bottom cavity interfaces than it is by gaps at the center of the cavity between samples. The systematic error in permittivity from modelling a sample with 20 μm height discrepancy was found to be $\sim$ 3% and the systematic error in permeability for a similar air gap along the center of the cavity was found to be only of the order of 1% however, there is again the introduction of oscillations at the Fabry-Perot frequencies. This oscillation error appears in both permeability and permittivity extractions, with the base value of the permittivity changing very little from the original value.

The results for relative permittivity and permeability of samples loaded with CIP ES are shown in Figs. 9 and 10. The relative permittivity and permeability of these samples at 200 MHz also increase logarithmically with percentage volume loading Fig. 11. A broad peak in the imaginary permeability from 1 GHz – 30 GHz, which increases in intensity with percentage loading, is also recorded. The absorption peak is primarily associated with the ferromagnetic resonance (FMR) of iron, which occurs at a frequency close to 2 GHz. The absorption peak is broadened by the presence of higher order spherical modes in the particles [25]–[28]. The size of these particles is such that the higher order spherical modes occur at frequencies similar to the FMR mode. Due to the particle size distribution of this CIP, these modes are also broadened and overlap the FMR mode to give a wide absorption band. It is possible that there are also conductive losses in these composites. Inter- and intra- particle conduction will contribute losses in permeability due to eddy currents [29]. These losses would be expected to increase with the square of frequency. However, since the size of the particles is so small, the eddy current loss may be assumed to be insignificant. In addition,

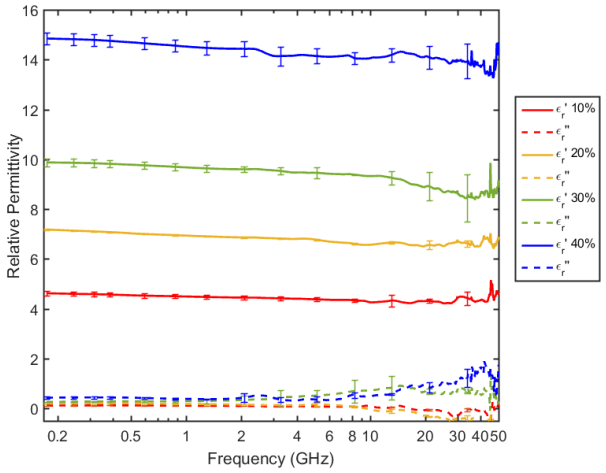

Fig. 9. Relative complex permittivity for CIP ES – Polyurethane composites with increasing percentage volume loading of CIP.

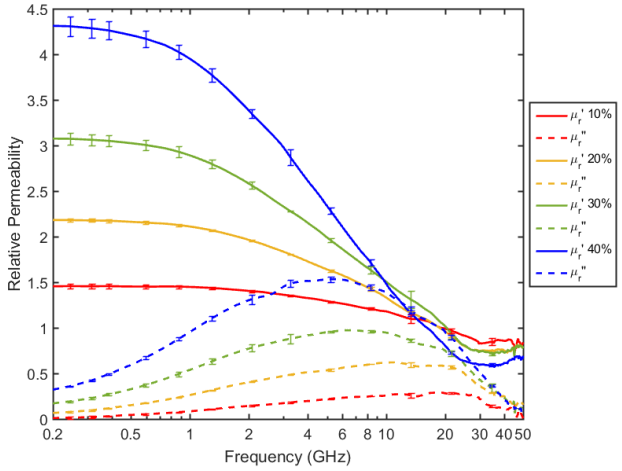

Fig. 10. Relative complex permeability for CIP ES – Polyurethane composites with increasing percentage volume loading of CIP.

the percentage loading of these composites is low, meaning the total eddy current losses in these composites should be negligible in comparison to the ferromagnetic losses.

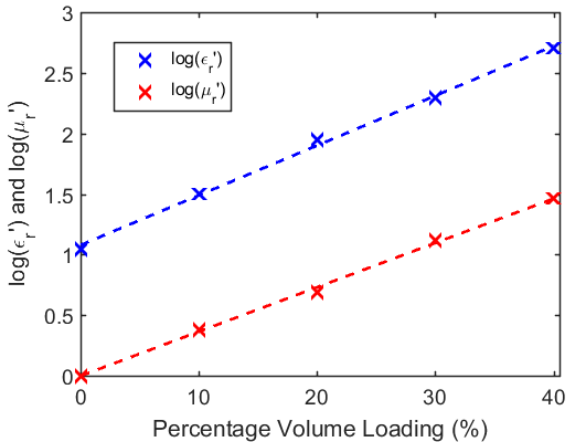

Fig. 11. Natural log of the real parts of relative permittivity and permeability at a frequency of 200 MHz, as a function of percentage volume loading for CIP – Polyurethane composites. The dashed lines show the results of a least squares, straight line fit to the data.

IV. Conclusion

A stripline geometry with a height of 3 mm, a cavity length of 20 mm and a central strip width of 3.82 mm has been fabricated with transition regions that have been optimized to favor impedance matching. S-parameter measurements taken with this device have been calibrated using an improvement on the triple-short technique which involves the use of seven 'short' readings rather than three. This calibration step allows the de-embedding of sample S-parameters from the stripline-sample system, accounting for the influence of the transitions from coaxial line to stripline. Fresnel theory has then been fitted to S-parameter data from these samples to extract relative complex permittivity for barium titanate – polyurethane composites with varying percentage loadings of barium titanate. The relative complex permittivity and permeability for carbonyl iron – polyurethane composites at different volume loadings of carbonyl iron is also determined. The results demonstrate that this method can be used to measure the effective permittivity and permeability for composite materials across the frequency range 200 MHz – 50 GHz and is viable for materials with refractive index at least as high as 8.

REFERENCES

[1] W. Barry, "A Broad-Band, Automated, Stripline Technique for the Simultaneous Measurement of Complex Permittivity and Permeability," *IEEE Trans. Microw. Theory Tech.*, vol. 34, no. 1, pp. 80–84, Jan 1986.

[2] A. M. Nicolson, "Broad-Band Microwave Transmission Characteristics from a Single Measurement of the Transient Response," *IEEE Trans. Instrum. Meas.*, vol. 17, no. 4, pp. 395–402, Dec 1968.

[3] A. M. Nicolson and G. F. Ross, "Measurement of the Intrinsic Properties of Materials by Time-Domain Techniques," *IEEE Trans. Instrum. Meas.*, vol. 19, no. 4, pp. 377–382, Nov 1970.

[4] W. B. Weir, "Automatic Measurement of Complex Dielectric Constant and Permeability," *Proc. IEEE*, vol. 62, no. 1, pp. 33–36, Jan 1974.

[5] N.-E. Belhadj-Tahar, A. Fourrier-Lamer, and H. de Chanterac, "Broadband simultaneous measurement of complex permittivity and permeability using a coaxial discontinuity," *IEEE Trans Microw. Theory Techn*, vol. 38, no. 1, pp. 1–7, Jan 1990.

[6] E. J. Vanzura, J. R. Baker-Jarvis, J. H. Grosvenor, and M. D. Janezic, "Intercomparison of permittivity measurements using the transmission/reflection method in 7-mm coaxial transmission lines," *IEEE Trans. Microw. Theory Tech.*, vol. 42, no. 11, pp. 2063–2070, Nov 1994.

[7] P. M. Jacquart and O. Acher, "Permeability measurement on composites made of oriented metallic wires from 0.1 to 18 GHz," *IEEE Trans. Microw. Theory Tech.*, vol. 44, no. 11, pp. 2116–2120, Nov 1996.

[8] J. Baker-Jarvis, M. D. Janezic, J. H. Grosvenor Jr., and R. G. Geyer, "Transmission/Reflection and Short-Circuit Line Methods for Measuring Permittivity," *NIST, Boulder, CO, USA, NIST Tech. Note*, vol. 1355, pp. 49–50, Dec 1993.

[9] J. Baker-Jarvis, M. D. Janezic, and J. Krupka, "Measurements of Coaxial Dielectric Samples Employing Both Transmission/Reflection and Resonant Techniques to Enhance Air-Gap Corrections," in *2006 Int. Conf. Microwaves, Radar Wirel. Commun.*, 2016, pp. 1–4.

[10] Y. Wang, I. Hooper, E. Edwards, and P. S. Grant, "Gap-Corrected Thin-Film Permittivity and Permeability Measurement With a Broadband Coaxial Line Technique," *IEEE Trans. Microw. Theory Tech.*, vol. 64, no. 3, pp. 1–7, Mar 2016.

[11] C. Chia-Hsing, L. Pao-Nan, and W. Sung-Mao, "The More Accurate Method to Extract Dielectric Constant and Loss Tangent of Insulated Material on Microwave Frequencies Chia-Hsing," in *IEEE 2005 Electron. Packag. Technol. Conf.*, 2005, pp. 806–809.

[12] S. B. Cohn, "Impedance of the Shielded-Strip Transmission Line," *Microw. Theory Tech.*, vol. 2, no. 2, pp. 52–57, 1954.

[13] T. Campbell, A. P. Hibbins, J. R. Sambles, and I. R. Hooper, "Broadband and low loss high refractive index metamaterials in the microwave regime," *Appl. Phys. Lett.*, vol. 102, no. 9, p. 091108, Mar 2013.

[14] S. Gómez, P. Quéffélec, A. Chevalier, A. C. Tarot, and A. Sharaiha, "Asymmetrical stripline based method for retrieving the electromagnetic properties of metamaterials Asymmetrical stripline based method for retrieving the electromagnetic properties of metamaterials," *J. Appl. Phys.*, vol. 113, p. 024912, Mar 2013.

[15] C. Jones, "Permittivity and permeability measurements using stripline resonator cavities-a comparison," *IEEE Trans. Instrum. Meas.*, vol. 48, no. 4, pp. 843–848, Aug 1999.

[16] L. Parke *et al.*, "Heavily loaded ferrite-polymer composites to produce high refractive index materials at centimetre wavelengths," *APL Mater.*, vol. 1, no. 4, p. 042108, Oct 2013.

[17] Anritsu Company, "Understanding VNA Calibration," p. 16, 2012.

[18] G. Hanson, J. Grimm, and D. Nyquist, "An improved de-embedding technique for the measurement of the complex constitutive parameters of materials using a stripline field applicator," *IEEE Trans. Instrum. Meas.*, vol. 42, no. 3, pp. 740–745, Jun 1993.

[19] D. A. Frickey, "Conversions Between S, 2, Y, h, ABCD, and T Parameters which are Valid for Complex Source and Load Impedances," vol. 30, no. 6, pp. 484–485, Feb 1994.

[20] K.-C. Cheng, C.-M. Lin, S.-F. Wang, S.-T. Lin, and C.-F. Yang, "Dielectric properties of epoxy resinbarium titanate composites at high frequency," *Mater. Lett.*, vol. 61, no. 3, pp. 757–760, May 2007.

[21] A. Patsidis and G. C. Psarras, "Dielectric behaviour and functionality of polymer matrix - Ceramic BaTiO 3 composites," *Express Polym. Lett.*, vol. 2, no. 10, pp. 718–726, Sep 2008.

[22] C. G. Raptis, A. Patsidis, and G. C. Psarras, "Electrical response and functionality of polymer matrix-titanium carbide composites," *Express Polym. Lett.*, vol. 4, no. 4, pp. 234–243, Feb 2010.

[23] A. Djordjević, D. Olćan, M. Stojilović, M. Pavlović, B. Kolundžija, and D. Tošić, "Causal Models of Electrically Large And Lossy Dielectric Bodies," *Electron. Energ.*, vol. 27, no. 2, pp. 221–234, Jun 2014.

[24] R. Simpkin, "Derivation of Lichtenecker's Logarithmic Mixture Formula From Maxwell's Equations," *IEEE Trans. Microw. Theory Tech.*, vol. 58, no. 3, pp. 545–550, Mar 2010.

[25] L. Z. Wu, J. Ding, H. B. Jiang, C. P. Neo, L. F. Chen, and C. K. Ong, "High frequency complex permeability of iron particles in a nonmagnetic matrix," *J. Appl. Phys.*, vol. 99, no. 8, p. 083905, Apr 2006.

[26] G. Viau, F. Fievet-Vincent, F. Fievet, P. Toneguzzo, F. Ravel, and O. Acher, "Size dependence of microwave permeability of spherical ferromagnetic particles," *J. Appl. Phys.*, vol. 81, no. 6, pp. 2749–2754, Nov 1997.

[27] A. N. Lagarkov, V. N. Semenenko, V. A. Chistyaev, and I. T. Iakubov, "High-frequency modes in magnetic spectra of carbonyl iron," *J. Magn. Magn. Mater.*, vol. 324, no. 21, pp. 3402–3405, Feb 2012.

[28] D. Mercier *et al.*, "Magnetic resonance in spherical Co-Ni and Fe-Co-Ni particles," *Phys. Rev. B Condens. Matter Mater. Phys.*, vol. 62, no. 1, pp. 532–544, Jul 2000.

[29] S. Konda, Y. Yoshida, and O. Ichinokura, "Eddy current loss evaluation of magnetic powder core based on electric and magnetic networks," *AIP Adv.*, vol. 7, no. 5, p. 056678, may 2017.